

SOLAR WIND TURBULENT SPECTRUM AT PLASMA KINETIC SCALES

O. ALEXANDROVA¹, C. LACOMBE¹, A. MANGENY¹, R. GRAPPIN^{2,3} AND M. MAKSIMOVIC¹

(Dated: November 15, 2012)
Draft version January 24, 2018

ABSTRACT

The description of the turbulent spectrum of magnetic fluctuations in the solar wind in the kinetic range of scales is not yet completely established. Here, we perform a statistical study of 100 spectra measured by the STAFF instrument on the Cluster mission, which allows to resolve turbulent fluctuations from ion scales down to a fraction of electron scales, i.e. from $\sim 10^2$ km to ~ 300 m. We show that for $k_{\perp}\rho_e \in [0.03, 3]$ (that corresponds approximately to the frequency in the spacecraft frame $f \in [3, 300]$ Hz), all the observed spectra can be described by a general law $E(k_{\perp}) \propto k_{\perp}^{-8/3} \exp(-k_{\perp}\rho_e)$, where k_{\perp} is the wave-vector component normal to the background magnetic field and ρ_e the electron Larmor radius. This exponential tail found in the solar wind seems compatible with the Landau damping of magnetic fluctuations onto electrons.

Subject headings: solar wind, plasma turbulence, kinetic scales

1. INTRODUCTION

In neutral, homogeneous and isotropic fluids, the turbulent fluctuations are unpredictable, but their statistics are predictable and universal (Frisch 1995); the turbulent spectra follow the power-law $\sim k^{-5/3}$ for any local conditions (k being the wave number). This empirical result was explained by Kolmogorov (Kolmogorov 1941) assuming self-similarity of the turbulent fluctuations between the energy injection scale and the dissipation one ℓ_d .

In the magnetized solar wind, collisions are very rare (the mean free path is of the order of 1 AU); the dissipation process at work and the dissipation length are not known precisely. Moreover, in a magnetized plasma, it is difficult to imagine self-similarity over all scales where turbulent fluctuations are observed, since there exist several spatial and temporal characteristic scales, such as the ion Larmor radius $\rho_i = \sqrt{2kT_{i\perp}/m_i}/(2\pi f_{ci})$, the ion inertia length $\lambda_i = c/\omega_{pi}$, the corresponding electron scales ρ_e, λ_e , and the ion and electron cyclotron frequencies f_{ci}, f_{ce} . At these scales, the dominant physical processes change, which affects the scaling of the energy transfer time and furthermore the energy transfer rate, leading to spectral shape changes.

The first clear spectral change appears at ion scales. At 1 AU, the ion scales are nearly equal, $\lambda_i \simeq \rho_i \simeq V/2\pi f_{ci}$, so it is difficult to determine which of these scales is responsible for the ion break. Independent measurements at different distances from the Sun, between 0.3 AU to 0.9 AU (Bourouaine et al. 2012), and a statistical study at 1 AU (Leamon et al. 2000) indicate that the spectral break is related to the ion inertia length λ_i . Nearly incompressible magnetic fluctuations cascading from the inertial range may undergo kinetic effects in the vicinity of the ion scales. At these scales, ion

temperature anisotropy instabilities occur (Gary et al. 2001) and can remove or inject energy in the turbulent cascade. However, for most of the solar wind observations, the plasma is stable (Matteini et al. 2007, 2011; Bale et al. 2009). The energy re-distribution among the fluid and kinetic degrees of freedom in the vicinity of ion scales is still a matter of debate and is probably at the origin of the spectral variations observed between 0.3 and 3 Hz in the satellite frame: the spectral index here varies between -4 and -2 (Leamon et al. 1998; Smith et al. 2006; Sahraoui et al. 2010). This spectral range is usually attributed to the ion dissipation range (Leamon et al. 1998, 1999, 2000; Smith et al. 2012) or to another fluid cascade, which may continue down to electron scales (Biskamp et al. 1996; Stawicki et al. 2001; Li et al. 2001; Galtier and Bhattacharjee 2003; Galtier and Buchlin 2007).

Between ion and electron scales, the fluctuations of the electron fluid form a small scale inertial range (Alexandrova et al. 2007, 2008), or, following the nomenclature of Smith et al. (2012), an electron inertial range. Here, indeed, a reproducible spectrum $\propto k_{\perp}^{-2.8}$ is observed (Alexandrova et al. 2009; Chen et al. 2010; Sahraoui et al. 2010). Approaching electron scales, one may expect to observe an electron dissipation range, as was suggested by Alexandrova (2008). At such small scales, there are only a few observations (Alexandrova et al. 2009; Sahraoui et al. 2010) and the descriptions are different. Larger statistical studies are needed to establish more firmly the properties of turbulent spectra at electron scales.

In this paper we present a large statistical study of magnetic spectra starting at ion scales and going beyond electron spatial scales. We use data from the STAFF instrument (Cornilleau-Wehrin et al. 1997) on the Cluster mission (Escoubet et al. 1997), which is able to measure such a range of scales. In a previous study, Alexandrova et al. (2009) described the electron inertial and the electron dissipation ranges separately: a power-law $\sim k^{-2.8}$ for the inertial range and a curved spectrum $\propto \exp(-\sqrt{k/k_0})$ for the dissipation range. This model is

¹ LESIA-Observatoire de Paris, CNRS, UPMC Université Paris 06, Université Paris-Diderot, 5 place J. Janssen, 92190 Meudon, France.

² LUTH-Observatoire de Paris, CNRS, Université Paris-Diderot, 5 place J. Janssen, 92190 Meudon, France

³ Ecole Polytechnique 91128 Palaiseau, France.

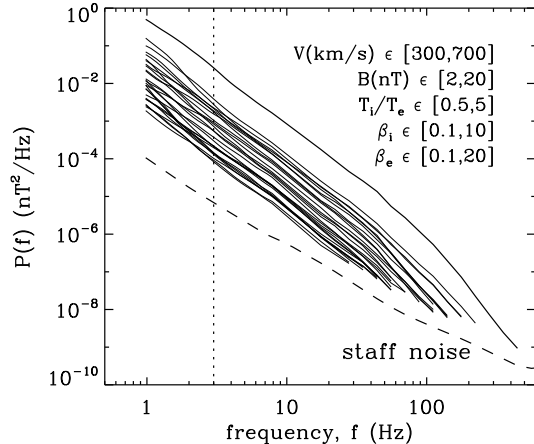


Figure 1. Frequency spectra with a signal to noise ratio greater than 3 measured by Cluster-1/STAFF in the free solar wind (for 27 intervals randomly chosen among 100). The dashed line shows the instrumental noise level. The vertical dotted line corresponds to $f = 3$ Hz. The legend indicates the variations of some solar wind parameters for the studied data set of 100 spectra: speed V , magnetic field B , temperature ratio and the ion and electron plasma β .

rather complicated and has a large number of free parameters. In the present study, we propose a single algebraic description for both ranges, namely, an exponential with a power-law pre-factor: $E(k_{\perp}) = Ak_{\perp}^{-\alpha} \exp(-k_{\perp} \ell_d)$. We find that this model describes well the totality of the observed spectra at scales smaller than λ_i and ρ_i and that its cut-off scale ℓ_d correlates with ρ_e . The power-law exponent α is found to be close to $-8/3$. This model (henceforth called “the *exp*-model”) has only one free parameter, the amplitude of the spectrum.

Previous authors (Sahraoui et al. 2010) have used a double power-law model with a break to fit the observations in the electron inertial and dissipation ranges. We have applied this model as well to our data, and we find that the first power-law exponent is consistent with the previous studies (Alexandrova et al. 2009; Chen et al. 2010) while the second exponent varies a lot. Despite the fact that the double power-law model has more free parameters than the exponential model used here, we find that it describes only 30% of the observed spectra and that the associated break scale does not present any clear correlation with an electron characteristic scale.

2. OBSERVATIONS

For our statistical study we select homogeneous intervals of 10 minutes (long enough to study kinetic scales) within the five years interval (2001–2005) of Cluster. We eliminate time intervals during which Cluster is magnetically connected to the bow-shock by using electrostatic wave spectrograms, which show clearly waves typical of the electron foreshock (Etcheto and Faucheux 1984; Lacombe et al. 1985), and by using the shock model described by Filbert and Kellogg (1979). For small angles Θ_{BV} between the interplanetary magnetic field \mathbf{B} and the solar wind velocity \mathbf{V} , Cluster is connected to the shock. Thus, our data set only contains intervals for which the angle $\Theta_{BV} > 60^\circ$. If the turbulent fluctuations have a phase speed $V_{\phi} \ll V$, Cluster detects by Doppler shift the fluctuations with $\mathbf{k} \parallel \mathbf{V}$. As \mathbf{B} and \mathbf{V} are

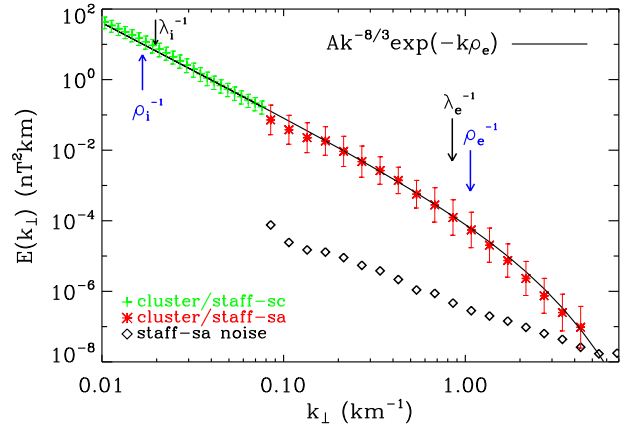


Figure 2. Fit of the most intense spectrum of Figure 1 with the *exp*-model. The spectrum was measured by Cluster-1/STAFF on 22/01/2004. Green crosses represent the SC measurements, red stars show the raw SA measurements without correction of the 1st three underestimated points, visible here around 0.1 km^{-1} . Diamonds indicate the STAFF-SA noise level. The blue arrows indicate inverse ion and electron Larmor radii, the black ones correspond to the inertial lengths. The solid line gives the *exp*-model $Ak^{-8/3} \exp(-k\rho_e)$.

quasi-perpendicular, Cluster measures fluctuations with $\mathbf{k} \perp \mathbf{B}$. We apply the Taylor hypothesis to get the wavenumber from the frequency, $k_{\perp} = 2\pi f/V$. However, about $\sim 10\%$ of the pre-selected intervals show the presence of right hand polarised whistlers in quasi-parallel propagation. For these waves the Taylor hypothesis is not applicable, because $V_{\phi} > V$. We discard these intervals in the present study. This data selection process gives us 100 intervals. Within this statistical sample, the plasma conditions vary as usually in the solar wind in fast and slow streams at 1 AU (see the legend of Figure 1).

Figure 1 shows the total Power Spectral Density (PSD) of magnetic fluctuations, for 27 intervals randomly chosen among 100, as a function of frequency in the spacecraft frame $P(f)$. These spectra are measured by the STAFF Search Coil sensor and analyzed onboard by the magnetic waveform unit (hereafter called SC) at $f \in [0.5, 9]$ Hz and by the Spectrum Analyser (hereafter called SA) at $f \geq 8$ Hz.

The spectra are analyzed only for the frequencies where the Signal to Noise Ratio (SNR) is larger than 3. The spectral parts below this threshold are not shown to avoid any erroneous interpretation. As one can see from Figure 1, this instrumental noise limit allows us to use data up to 30–400 Hz, depending on the turbulence intensity (i.e., for the most intense spectrum, we have valid observations up to 400 Hz). The analyzed range of frequencies corresponds to $f \in]f_{ci}, f_{ce}]$.

A poor calibration of the first 3 frequencies of SA (at 8, 11 and 14 Hz) [Y. de Conchy and N. Cornilleau, private communication, 2011], was corrected by an interpolation of these points between the highest SC frequency and the 4th point of the SA spectra. The linear interpolation between $\log_{10} P(f)$ and $\log_{10} f$ is possible as far as the spectra follow a power-law at these frequencies. An example of a raw spectrum without the correction can be found in Figure 2.

3. ALGEBRAIC DESCRIPTION OF TURBULENT SPECTRA AT SCALES SMALLER THAN ρ_i AND λ_i .

3.1. Exponential model

Here we propose a model to describe the whole turbulent spectrum at scales smaller than ρ_i and λ_i and down to a fraction of the electron scales with the smaller possible number of parameters, namely an exponential with a characteristic scale ℓ_d and with a power-law pre-factor

$$E(k_{\perp}) = Ak_{\perp}^{-\alpha} \exp(-k_{\perp} \ell_d). \quad (1)$$

This *exp*-model has three free parameters: the amplitude A , the spectral index α and the cut-off or "dissipation" scale ℓ_d .

We start by fitting the model (1) to the 100 observed spectra (with a signal to noise ratio > 3 , as explained in section 2) for k_{\perp} corresponding to $f > 3$ Hz (see vertical dotted line in Figure 1), assuming that the three parameters have independent variations.

Figure 2 gives the fit with the most intense spectrum of Figure 1 as a function of the wave-number $P(k_{\perp}) = P(f)V/2\pi$, which is determined using the Taylor hypothesis and the energy conservation law $\int P(k_{\perp})dk_{\perp} = \int P(f)df$. Green crosses show the Morlet wavelet spectrum (Torrence and Compo 1998) of STAFF-SC measurements. Red stars display the STAFF-SA data for the same time period. (In this plot we keep the 3 first poorly calibrated data points, one can see them around $k = 0.1 \text{ km}^{-1}$ and compare with the result of the interpolation in Figure 1). The error bars are estimated from the variance over 10 minutes of the PSD at each frequency (Alexandrova et al. 2010). This spectrum is valid up to $\simeq 400 \text{ Hz}$, which gives us the maximum wave-vector $k \sim 4 \text{ km}^{-1}$ (while $1/\rho_e \simeq 1 \text{ km}^{-1}$). This is the smallest scale ever measured with a good sensitivity at 1 AU in the solar wind. The *exp*-model (1) fitting is shown by the black solid line. The parameters of the fit in this case are $\alpha = 2.70 \pm 0.15$ and $\ell_d = (0.90 \pm 0.25) \text{ km}$, while $\rho_e = (0.95 \pm 0.05) \text{ km}$.

Figure 3 summarizes the results of the fitting for the 100 spectra. Panel (a) shows the histogram of the spectral index, $\alpha = 2.63 \pm 0.15$, the error being the standard deviation of the mean. Note that $\langle \alpha \rangle \simeq 8/3$. It appears that the variations of α and ℓ_d are not independent since the dispersion in α is due to the variations of the cut-off scale ℓ_d as observed in Figure 3b. A linear fit gives $\ell_d(\text{km}) = 12.9 - 4.4\alpha$, i.e.

$$\alpha = 2.9 - \ell_d/4.4 \quad (2)$$

i.e. if ℓ_d was small, α would be approximately equal to 2.9, a value close to the one found by Alexandrova et al. (2009).

On the other hand, the variations of ℓ_d are related to the variations of the electron Larmor radius, $\ell_d \sim 1.35\rho_e$, as shown in Figure 3c, with a relatively high correlation coefficient of 0.70. Figure 3d shows a positive but much weaker correlation of 0.34 between the dissipation scale ℓ_d and the electron inertia length λ_e .

The results presented in Figure 3 suggest that within the framework of the exponential model there is only one free parameter, the amplitude of the turbulent spectra, A , and the observed spectra can be described approxi-

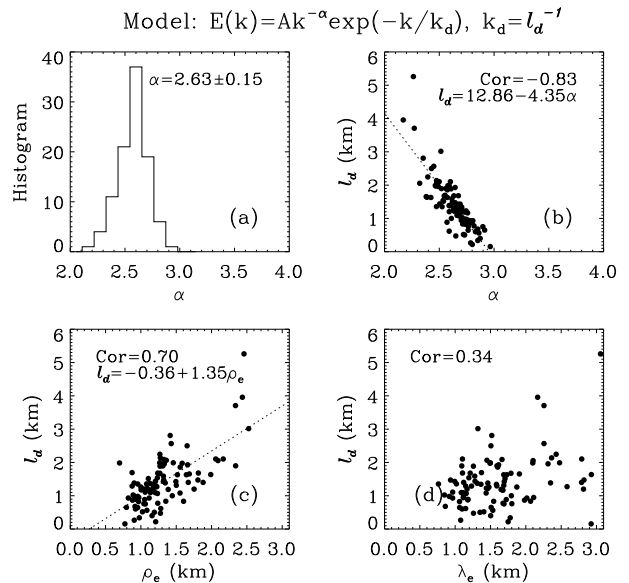


Figure 3. Results of the fitting with the *exp*-model for the 100 observed spectra: (a) histograms on the spectral index α ; (b) cut-off scale ℓ_d as a function of α ; (c) ℓ_d as a function of the electron Larmor radius ρ_e and (d) ℓ_d as a function of the electron inertial length λ_e .

mately by

$$E(k_{\perp}) \simeq Ak_{\perp}^{-8/3} \exp(-k_{\perp} \rho_e). \quad (3)$$

We verify this point in Figure 4, where we superpose the 100 spectra analyzed here with the 7 spectra covering fluid and kinetic scales from (Alexandrova et al. 2009). The spectra are shifted vertically by a parameter E_0 (a relative spectral level), in the same way as in Fig. 2 of (Alexandrova et al. 2009). The superposition of the 107 spectra is nice, which indicates the generality of the turbulent spectrum $E(k_{\perp})$ in the solar wind: it follows $\propto k_{\perp}^{-5/3}$ at MHD scales and $\propto k_{\perp}^{-8/3} \exp(-k_{\perp} \rho_e)$ at scales smaller than the ion kinetic scales λ_i and ρ_i (i.e. $k\rho_e \geq 0.03$). The bottom panel shows the 100 spectra $E(k_{\perp} \rho_e)$ compensated by a function $F = (k_{\perp} \rho_e)^{8/3} \exp(k_{\perp} \rho_e)$ for $k\rho_e \geq 0.03$: the resulting spectra are flat, indicating that the *exp*-model with one free parameter describes well all the turbulent spectra in the solar wind at these scales and is valid for nearly 2 decades in wave numbers. Note that a damping length ℓ_d variation of more than 20% with respect to the mean ρ_e values results in a strong departure of the compensated spectra.

The amplitude A of the turbulent spectra (related to the parameter E_0) is found to be correlated with the ion thermal pressures nkT_i , as within the MHD range of turbulence (Grappin et al. 1990), and with the ion temperature anisotropy $T_{i\perp}/T_{i\parallel}$ (not shown). Other plasma parameters seem to be less important, but still it is impossible to exclude completely the influence of the magnetic and kinetic energies in the solar wind (paper in preparation).

3.2. Break model

Is there another simple model which represents well the observations with a small number of free parameters?

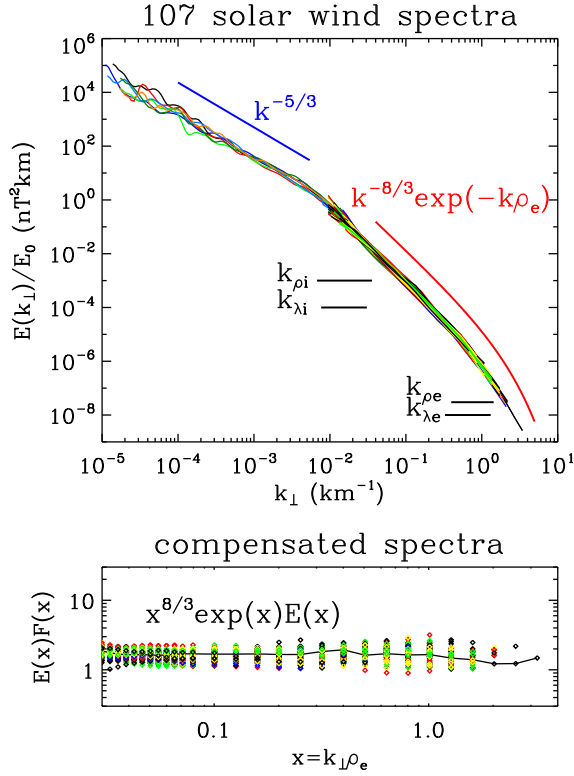


Figure 4. Upper panel: 107 superposed solar wind spectra, the 100 spectra in the kinetic range analysed in this paper and the 7 spectra covering fluid and kinetic scales from (Alexandrova et al. 2009), the constant being $E_0 \in [0.4, 95]$. All spectra have the signal to noise ratio greater than 3, as in Figure 1. The blue line indicates $\propto k_{\perp}^{-5/3}$ and the red line shows $\propto k_{\perp}^{-8/3} \exp(-k_{\perp} \rho_e)$, that represents well all the spectra. Bottom panel: the diamonds show 100 compensated spectra $E(k_{\perp} \rho_e) \cdot F(k_{\perp} \rho_e)$, with $F(k_{\perp} \rho_e) = (k_{\perp} \rho_e)^{8/3} \exp(k_{\perp} \rho_e)$, for $k_{\perp} \rho_e \geq 0.03$. The solid line denotes the most intense compensated spectrum.

Let us compare the turbulent spectra within the electron inertial and dissipation ranges (i.e. scales smaller than ρ_i and λ_i) with the double power-law or *break*-model

$$\tilde{E}(k_{\perp}) = A_1 k_{\perp}^{-\alpha_1} (1 - H(k_{\perp} - k_b)) + A_2 k_{\perp}^{-\alpha_2} H(k_{\perp} - k_b), \quad (4)$$

$H(k_{\perp} - k_b)$ being the Heaviside function, k_b the wave number of the break scale $\ell_b = 1/k_b$, $A_{1,2}$ the amplitudes of the two power-law functions with spectral indices $\alpha_{1,2}$ on both sides of k_b . This model has five free parameters. Note that equation (4) is not differentiable for $k = k_b$. Near k_b the turbulent level has to be the same on both sides. Thus, k_b can be determined by the four other parameters of the model

$$\log_{10} k_b = \frac{\log_{10}(A_1/A_2)}{\alpha_1 - \alpha_2}. \quad (5)$$

Iterations to find the model parameters with condition (5) converge to different results, depending on the initial k_b . Therefore, minimising the error of the fit over k_b is needed, so that finally the model has still five free parameters.

We apply this *break*-model to the 100 observed spectra within the same k_{\perp} -range as was done for the *exp*-model. Despite the fact that the *break*-model has more free pa-

rameters than the exponential model, we find that it can be applied only to 30 spectra; for the 70 other spectra there is no solution with condition (5) verified, indicating the absence of a clear break point, or, for a part of these spectra, not enough data points to isolate the second power-law.

Model: $E(k) = A_1 k^{-\alpha_1} (1 - H(k - k_b)) + A_2 k^{-\alpha_2} H(k - k_b)$, $k_b = \ell_b^{-1}$

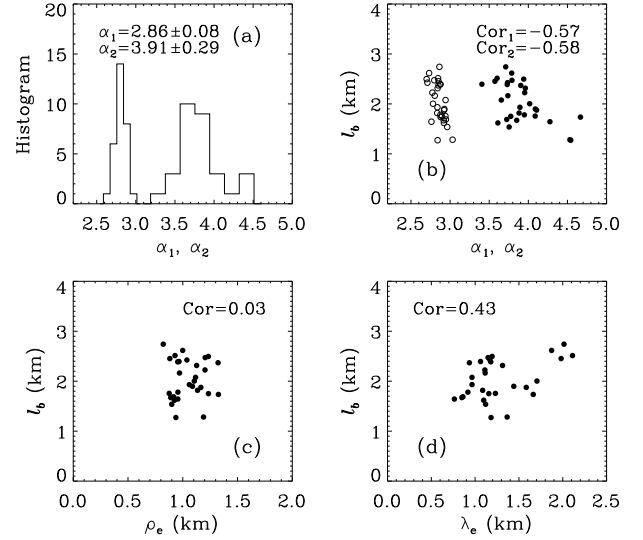


Figure 5. same format as Figure 3, but for the parameters of the *break*-model determined from the fitting with 30 spectra, i.e. (a) histograms on the spectral indices; (b) break scale ℓ_b as a function of α_1 (open circles) and α_2 (filled circles); (c) ℓ_b as a function of the electron Larmor radius ρ_e and (d) ℓ_b as a function of the electron inertial length λ_e .

Figure 5 summarizes the parameters of the *break*-model determined from the fitting of the 30 spectra. For these spectra, the condition (5) is verified. Panel (a) shows histograms of the spectral indices: the mean values are $\alpha_1 = 2.86 \pm 0.08$, $\alpha_2 = 3.91 \pm 0.29$. Note the narrow dispersion of the spectral index α_1 . It is close to α , when ℓ_d is negligible (see eq. (2)) so confirming the spectrum between ion and electron scales found by Alexandrova et al. (2009). So we can fix one of the parameters of the model. The second exponent α_2 has a large dispersion, not found to be controlled by any plasma parameter. The values of the spectral indices are correlated to the position of the break scale ℓ_b (see panel b). Figure 5c shows ℓ_b as a function of ρ_e . No correlation is observed. Figure 5d shows ℓ_b as a function of λ_e : the correlation is positive but weak ($\simeq 0.43$). From the comparison of the observed turbulence spectra at plasma kinetic scales with the *break*-model, one may conclude that this model has one fixed parameter, another is fixed by the condition (5), the other 3 parameters are free, not found to be determined by plasma parameters.

It is important to note that the errors of the fit of the *break* and *exp*-models are of the same order. Figure 6 shows an example of a solar wind spectrum (black lines) fitted with both models, with the least mean square distance between the observed spectra and the fit, Δ^2 , given in the caption; the insert shows histograms of Δ_{exp}^2 (red) for 100 spectra and Δ_{break}^2 (blue) for 30 spectra: the same mean values of the histograms are observed. This

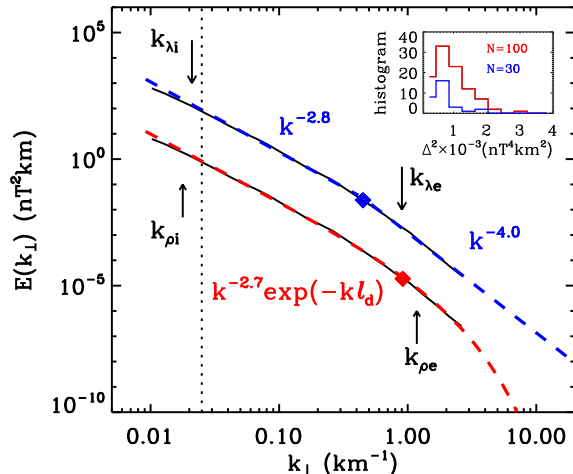


Figure 6. Example of an observed spectrum (lower black line) compared with $E(k) \sim k^{-2.7} \exp(-k\ell_d)$ (red dashed line), with ℓ_d^{-1} marked by a red diamond; the error of the fit is $\Delta_{exp}^2 = 1.8 \times 10^{-3}$ ($\text{nT}^4 \text{km}^2$). The same spectrum, shifted by a factor 10^2 and compared with $E(k) \sim k^{-2.8}$ below the break shown by a blue diamond, and with $k^{-4.0}$ above it (blue dashed line); here $\Delta_{break}^2 = 1.9 \times 10^{-3}$ ($\text{nT}^4 \text{km}^2$). Ion and electron characteristic scales are marked by arrows; a vertical dotted line indicates the beginning of the k -domain where the fits are performed. Insert: histograms of the fitting errors, Δ_{exp}^2 (red, for 100 spectra) and Δ_{break}^2 (blue, for 30 spectra).

leaves us free to choose the model, based on other criteria than goodness of the fit, namely, on the number of degrees of freedom of the model and on the number of described cases.

4. DISCUSSION AND CONCLUSION

The *exp*-model $E(k_\perp) = Ak_\perp^{-8/3} \exp(-k_\perp \rho_e)$ proposed in this study provides a single algebraic description of the solar wind spectrum at scales smaller than the ion characteristic scales, λ_i and ρ_i , and going beyond the electron scales (i.e. within the electron inertial and dissipation ranges). This model describes well the totality of the observed spectra and has only one free parameter – the amplitude A of the spectrum. The amplitude seems to be a function of the ion thermal pressure and the ion temperature anisotropy in the solar wind. However, it is difficult to exclude the role of the magnetic and kinetic energies: more work is needed to determine the exact relationship between the amplitude of the turbulent spectrum and the energy budget in the solar wind.

The spectral index close to $-8/3$ observed in the solar wind at scales smaller than ion characteristic scales is in agreement with quasi-bidimensional strong Electron MHD turbulence ($k_\perp \gg k_\parallel$) when parallel cascade is weak (Galtier et al. 2005). Recently, the same spectral index was found as well in strong kinetic Alfvén turbulence (Boldyrev and Perez 2012).

In usual fluid turbulence, the far dissipation range is described by $E(k) \sim k^3 \exp(-ck\ell_d)$ (with $c \simeq 7$) (Chen et al. 1993). This is due to the resistive damping rate $\propto k^2$ valid in a collisional fluid, which gives an exponential spectral tail. In the collisionless plasma of the solar wind there is no resistive damping, and thus

this coincidence deserves an explanation.

Howes et al. (2011) consider a model (“weakened cascade model”) which includes the nonlinear transfer of energy from large to small scales in Fourier space and the damping of kinetic Alfvén waves (KAW’s). For completeness, we discuss now this model in some detail. The model reads for the magnetic energy b^2 at scale k :

$$\partial_t b_k^2 = -k_\perp \partial_k \epsilon - 2\gamma b_k^2 + S \quad (6)$$

with ϵ being the magnetic energy transfer rate, S being the source term. The damping term $2\gamma b_k^2$ is obtained by linearizing the Vlasov-Maxwell equations in the gyrokinetic limit ($k_\parallel \ll k_\perp$, with frequencies $f \ll f_{ci}$). In the limit $k\rho_i \gg 1$, this gives

$$\gamma \simeq k_\parallel V_a (k_\perp \rho_i)^2, \quad (7)$$

see eq. (63) in (Howes et al. 2006). To complete the model, we must write down the expression for the magnetic energy flux ϵ . This is given by

$$\epsilon = b^2/\tau = k_\perp u b^2 \quad (8)$$

where $\tau = 1/k_\perp u$ is the nonlinear time and u the velocity fluctuation. At MHD scales $k_\perp \rho_i \ll 1$, we have for Alfvén waves $u \simeq b$, but at small scales $k_\perp \rho_i \geq 1$, we have for KAW $u/b \simeq k_\perp \rho_i$, see eq. (3) in (Howes et al. 2011). Using these expressions in eq. (6) and (8), one obtains scaling laws for the magnetic energy spectrum as stationary solutions of the transfer equation (6), neglecting the damping and source terms. The spectral laws are respectively $E_k \propto k_\perp^{-5/3}$ at large scales and $E_k \propto k_\perp^{-7/3}$ between ion and electron scales. When taking into account the damping term, Howes et al. (2011) obtain numerically the same spectral laws, with a final curved tail at scales smaller than electron scales. Superficially, this spectrum thus resembles the analytic form which we have found to be valid to describe the solar wind turbulence.

We last remark that the damping term in the model of Howes et al. (2011) for $k_\perp \rho_i \gg 1$ is (see eq. (7)) of the form $\gamma \propto k_\parallel k_\perp^2$. Taking into account the assumption of critical balance $\tau = \tau_A$ (i.e. $k_\perp u = k_\parallel V_A$) (Goldreich and Sridhar 1995), with τ_A the Alfvén time and V_A the Alfvén speed, and the spectral index $-7/3$ (i.e. $u \sim k_\perp^{-2/3}$), one gets $k_\parallel \propto k_\perp^{1/3}$. Therefore, the damping term takes the form $\gamma \propto k_\perp^{2+1/3}$. The exponent of the damping rate is thus very close to the k^2 scaling of the Laplacian viscous term, which is known to lead in hydrodynamical turbulence to an exponential tail in the dissipation range.

This model does not take into account the cyclotron damping. So, while the proposed phenomenology may explain the exponential tail of the k_\perp -spectrum studied here, it cannot describe more isotropic wave vectors, which might be present as well in the solar wind. It is possible that the dissipation mechanism could also be due to electron-cyclotron absorption of oblique short-wavelength whistler waves, or even of lower-hybrid waves. More observations under different field-to-flow angles Θ_{BV} are needed within the electron inertial and dissipation ranges to address this point.

To build a realistic model of the dissipation in the solar wind we need to resolve still an open question

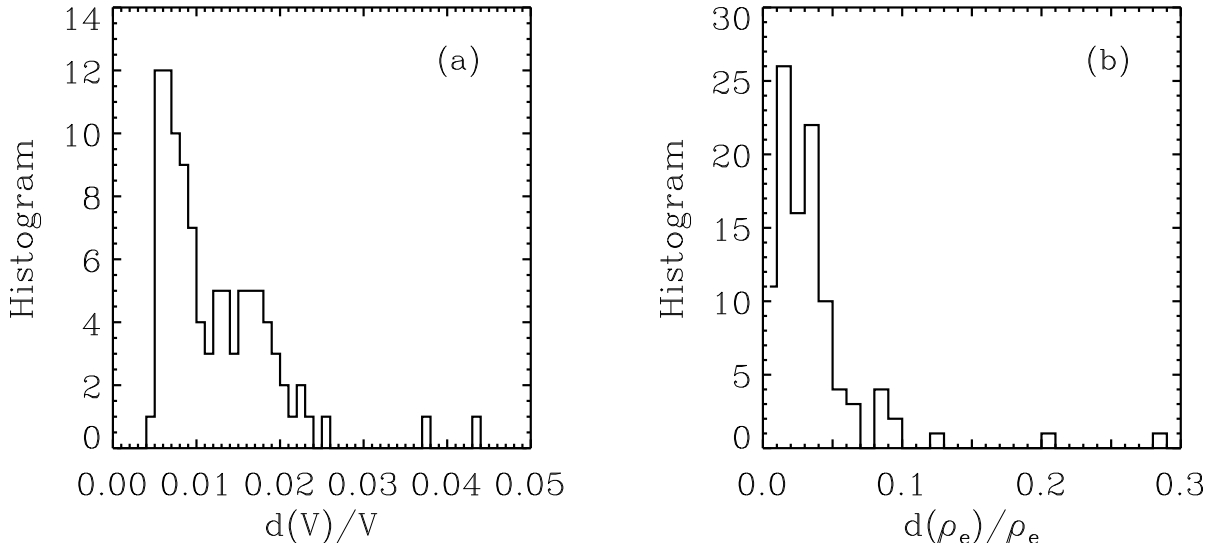


Figure 7. Histogram of the variability of the solar wind speed V during 10 minutes, for a sample of 100 intervals (left panel). Right panel : histogram of the variability of the electron gyroradius ρ_e .

on the nature of the turbulent fluctuations. Some authors argue that the electron inertial range is a whistler mode turbulence (Saito et al. 2010; Narita and Gary 2010), others suggest KAW turbulence (Bale et al. 2005; Schekochihin et al. 2009; Sahraoui et al. 2010; Salem et al. 2012), or a combination of both types of linear waves (Podesta and Gary 2011). The model of Howes et al. (2011), described above is based on KAW turbulence as well. However, it is still not clear whether we can describe turbulence in the solar wind as a mixture

of linear waves (weak turbulence) which will dissipate homogeneously in space (or in the plane perpendicular to \mathbf{B}), or if it is a strong turbulence with dissipation restricted to intermittent coherent structures. What is the topology of these structures – current sheets, shocks or coherent vortices?

In the present study we have limited ourselves to observations of the spectral shape in the electron inertial and dissipation ranges. Our results give observational constraints for future theoretical models.

APPENDIX

PLASMA PARAMETERS VARIATIONS DURING THE SPECTRA INTEGRATION TIME

One could argue that the exponential bending found in the k -spectra of the magnetic fluctuations is due to variations of the solar wind speed V or of the gyroradius ρ_e during the 10 minutes of each considered interval. Indeed, each k -spectrum is obtained with an average $P(f)$ over 150 frequency spectra, itself shifted in the k -domain with the average V . The standard deviation dV over 10 minutes is very small. Figure 7(a) displays the histogram of the ratio dV/V : 91% of the 100 considered intervals have $dV/V < 0.02$. Thus, the shift of $P(f)$ in the k -domain with the average V cannot change the spectral bending. Similarly, the standard deviation $d(\rho_e)$ over 10 minutes is small. Figure 7(b) displays the histogram of the ratio $d(\rho_e)/\rho_e$: 96% of the 100 considered intervals have $d(\rho_e)/\rho_e < 0.1$. Thus, the use of the average ρ_e for an interval, in place of the exact ρ_e for each of the 150 k -spectra, cannot produce the observed bending which covers a wide range of k , and cannot smooth a possible spectral break.

LOG-SPACED FREQUENCIES OF THE CLUSTER/STAFF-SA INSTRUMENT

Another argument against the observed spectral bending could be that it is an artefact due to the logarithmic frequency binning of the Spectrum Analyser (SA) on Cluster.

Indeed, the centre frequency of the output channels of SA are distributed logarithmically (between 8.8 Hz and 3.56 kHz), and each channel has a bandpass proportional to its centre frequency, $2df = 26f/100$. As the onboard waveforms used by SA are lost, we have no way to check whether a different frequency binning would give different frequency spectra. We only make a crude comparison between an analytical frequency spectrum $P_A(f)$ and the same spectrum integrated by a trapeze method in the logarithmic frequency bands of SA, $P_T(f)$. Note that the trapeze integration has to be made on the logarithms of $P_A(f)$ because the gain of the STAFF-SA receivers is proportional to the logarithm of the power. Figure 8 gives the results of this comparison for a spectral break model (with two spectral indices $\alpha_1 = 2.8$, $\alpha_2 = 4$, left panel) and for an exponential model (right panel) $P_A(f) = f^{-2.7} \exp(-f/f_0)$, with $f_0 \simeq 115$ Hz. The solid lines give $P_A(f)$, and the crosses give $P_T(f)$ in the 18 lowest frequencies of SA. It is clear that the trapeze integration in logarithmic channels does not change the shape of the spectra. The ratio $R = P_T/P_A$ is very close to unity: 1.02 to 1.03. There is thus a slight systematic overestimation of the spectrum by the trapeze integration in logarithmic bands. This overestimation (2 to 3%) cannot increase the downward bending of the spectrum. We conclude that the logarithmic frequency binning of the Spectrum Analyser cannot smooth a possible spectral break,

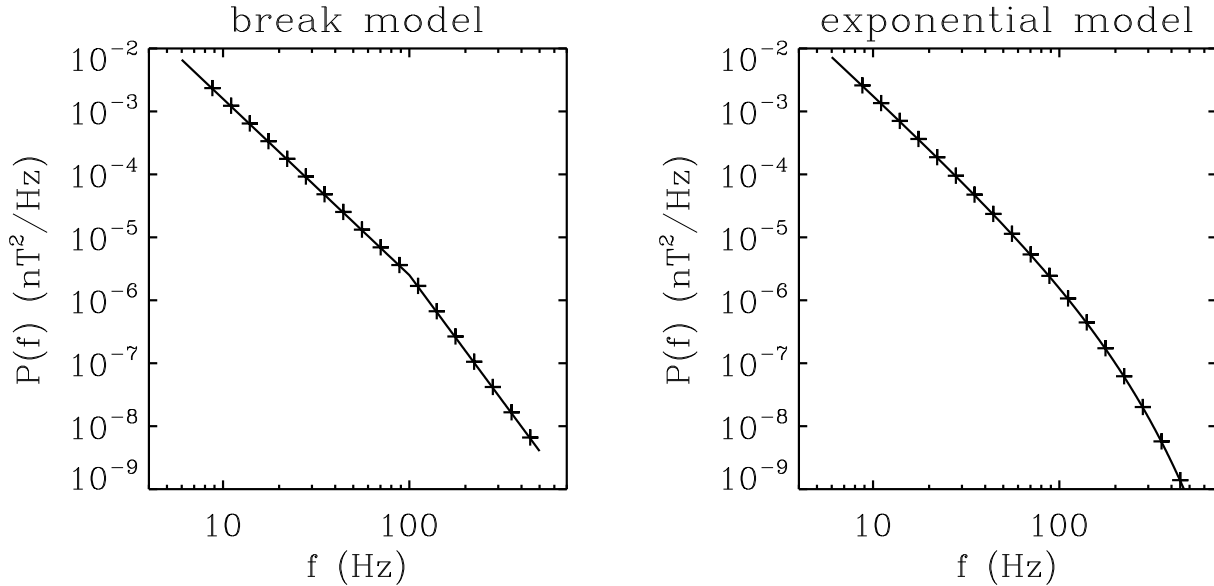


Figure 8. Comparison between an analytic power spectrum $P_A(f)$ (solid line) and the power spectrum $P_T(f)$ (crosses) calculated by a trapeze integration of $P_A(f)$ with the logarithmic frequency binning of the Spectrum Analyser ($2df = 26\%$), for the two models discussed in the paper. The difference between $P_T(f)$ and $P_A(f)$ is less than 3%.

and cannot produce an artificial downward bending of the spectra.

REFERENCES

- O. Alexandrova. Solar wind vs magnetosheath turbulence and Alfvén vortices. *Nonlinear Processes in Geophysics*, 15:95–108, Feb. 2008.
- O. Alexandrova, V. Carbone, P. Veltri, and L. Sorriso-Valvo. Solar wind Cluster observations: Turbulent spectrum and role of Hall effect. *Planet. Space Sci.*, 55:2224–2227, Dec. 2007. doi:10.1016/j.pss.2007.05.022.
- O. Alexandrova, V. Carbone, P. Veltri, and L. Sorriso-Valvo. Small-Scale Energy Cascade of the Solar Wind Turbulence. *Astrophys. J.*, 674:1153–1157, Feb. 2008. doi:10.1086/524056.
- O. Alexandrova, J. Saur, C. Lacombe, A. Mangeney, J. Mitchell, S. J. Schwartz, and P. Robert. Universality of Solar-Wind Turbulent Spectrum from MHD to Electron Scales. *Physical Review Letters*, 103(16):165003–+, Oct. 2009. doi:10.1103/PhysRevLett.103.165003.
- O. Alexandrova, J. Saur, C. Lacombe, A. Mangeney, S. J. Schwartz, J. Mitchell, R. Grappin, and P. Robert. Solar wind turbulent spectrum from MHD to electron scales. *12th Int. Solar Wind Conference, AIP Conference Proceedings*, 1216:144–147, Mar. 2010. doi:10.1063/1.3395821.
- S. D. Bale, P. J. Kellogg, F. S. Mozer, T. S. Horbury, and H. Reme. Measurement of the Electric Fluctuation Spectrum of Magnetohydrodynamic Turbulence. *Physical Review Letters*, 94(21):215002–+, June 2005. doi:10.1103/PhysRevLett.94.215002.
- S. D. Bale, J. C. Kasper, G. G. Howes, E. Quataert, C. Salem, and D. Sundkvist. Magnetic Fluctuation Power Near Proton Temperature Anisotropy Instability Thresholds in the Solar Wind. *Physical Review Letters*, 103(21):211101–+, Nov. 2009. doi:10.1103/PhysRevLett.103.211101.
- D. Biskamp, E. Schwarz, and J. F. Drake. Two-Dimensional Electron Magnetohydrodynamic Turbulence. *Physical Review Letters*, 76:1264–1267, Feb. 1996. doi:10.1103/PhysRevLett.76.1264.
- S. Boldyrev and J. C. Perez. Spectrum of Kinetic-Alfvén Turbulence. *ApJ*, 758:L44, Oct. 2012. doi:10.1088/2041-8205/758/2/L44.
- S. Bourouaine, O. Alexandrova, E. Marsch, and M. Maksimovic. On Spectral Breaks in the Power Spectra of Magnetic Fluctuations in Fast Solar Wind between 0.3 and 0.9 AU. *ApJ*, 749:102, Mar. 2012. doi:10.1088/0004-637X/749/2/102.
- C. H. K. Chen, T. S. Horbury, A. A. Schekochihin, R. T. Wicks, O. Alexandrova, and J. Mitchell. Anisotropy of Solar Wind Turbulence between Ion and Electron Scales. *Physical Review Letters*, 104(25):255002–+, June 2010. doi:10.1103/PhysRevLett.104.255002.
- S. Chen, G. Doolen, J. R. Herring, R. H. Kraichnan, S. A. Orszag, and Z. S. She. Far-dissipation range of turbulence. *Physical Review Letters*, 70:3051–3054, May 1993. doi:10.1103/PhysRevLett.70.3051.
- N. Cornilleau-Wehrin et al. The Cluster Spatio-Temporal Analysis of Field Fluctuations (STAFF) Experiment. *Space Science Reviews*, 79:107–136, Jan. 1997.
- C. P. Escoubet, R. Schmidt, and M. L. Goldstein. Cluster - Science and Mission Overview. *Space Science Reviews*, 79:11–32, Jan. 1997. doi:10.1023/A:1004923124586.
- J. Etcheto and M. Faucheux. Detailed study of electron plasma waves upstream of the earth’s bow shock. *J. Geophys. Res.*, 89:6631–6653, Aug. 1984. doi:10.1029/JA089iA08p06631.
- P. C. Filbert and P. J. Kellogg. Electrostatic noise at the plasma frequency beyond the earth’s bow shock. *J. Geophys. Res.*, 84:1369–1381, Apr. 1979. doi:10.1029/JA084iA04p01369.
- U. Frisch. *Turbulence. The legacy of A.N. Kolmogorov*. Cambridge: Cambridge University Press, 1995.
- S. Galtier and A. Bhattacharjee. Anisotropic weak whistler wave turbulence in electron magnetohydrodynamics. *Physics of Plasmas*, 10:3065, Aug. 2003.
- S. Galtier and E. Buchlin. Multiscale Hall-Magnetohydrodynamic Turbulence in the Solar Wind. *Astrophys. J.*, 656:560–566, Feb. 2007. doi:10.1086/510423.
- S. Galtier, A. Pouquet, and A. Mangeney. On spectral scaling laws for incompressible anisotropic magnetohydrodynamic turbulence. *Physics of Plasmas*, 12(9):092310, Sept. 2005. doi:10.1063/1.2052507.
- S. P. Gary, R. M. Skoug, J. T. Steinberg, and C. W. Smith. Proton temperature anisotropy constraint in the solar wind: ACE observations. *Geophys. Res. Lett.*, 28:2759–2762, July 2001. doi:10.1029/2001GL013165.

- P. Goldreich and S. Sridhar. Toward a theory of interstellar turbulence. 2: Strong alfvénic turbulence. *The Astrophysical Journal*, 438: 763–775, Jan. 1995. doi:10.1086/175121.
- R. Grappin, A. Mangeney, and E. Marsch. On the origin of solar wind MHD turbulence - HELIOS data revisited. *J. Geophys. Res.*, 95: 8197–8209, June 1990. doi:10.1029/JA095iA06p08197.
- G. G. Howes, S. C. Cowley, W. Dorland, G. W. Hammett, E. Quataert, and A. A. Schekochihin. Astrophysical Gyrokinetics: Basic Equations and Linear Theory. *ApJ*, 651:590–614, Nov. 2006. doi:10.1086/506172.
- G. G. Howes, J. M. Tenbarge, and W. Dorland. A weakened cascade model for turbulence in astrophysical plasmas. *Physics of Plasmas*, 18(10):102305, Oct. 2011. doi:10.1063/1.3646400.
- A. N. Kolmogorov. The local structure of turbulence in incompressible viscous fluid for very large Reynolds numbers. *Dokl. Akad. Nauk SSSR*, 30:9–13, 1941.
- C. Lacombe, A. Mangeney, C. C. Harvey, and J. Scudder. Electron Plasma Waves Upstream of the Earth’s Bow Shock. *J. Geophys. Res.*, 90:73–94, 1985. doi:10.1029/JA090iA01p00073.
- R. J. Leamon, C. W. Smith, N. F. Ness, W. H. Matthaeus, and H. K. Wong. Observational constraints on the dynamics of the interplanetary magnetic field dissipation range. *J. Geophys. Res.*, 103(12):4775, mar 1998.
- R. J. Leamon, C. W. Smith, N. F. Ness, and H. K. Wong. Dissipation range dynamics: Kinetic Alfvén waves and the importance of electron beta β_e . *J. Geophys. Res.*, 104(13):22331–22344, Oct. 1999. doi:10.1029/1999JA900158.
- R. J. Leamon, W. H. Matthaeus, C. W. Smith, G. P. Zank, D. J. Mullan, and S. Oughton. MHD-driven Kinetic Dissipation in the Solar Wind and Corona. *The Astrophysical Journal*, 537:1054–1062, July 2000. doi:10.1086/309059.
- H. Li, S. P. Gary, and O. Stawicki. On the dissipation of magnetic fluctuations in the solar wind. *Geophysical Research Letters*, 28: 1347–1350, Apr. 2001. doi:10.1029/2000GL012501.
- L. Matteini, S. Landi, P. Hellinger, F. Pantellini, M. Maksimovic, M. Velli, B. E. Goldstein, and E. Marsch. Evolution of the solar wind proton temperature anisotropy from 0.3 to 2.5 AU. *Geophys. Res. Lett.*, 34:L20105, Oct. 2007. doi:10.1029/2007GL030920.
- L. Matteini, P. Hellinger, S. Landi, P. M. Trávníček, and M. Velli. Ion Kinetics in the Solar Wind: Coupling Global Expansion to Local Microphysics. *Space Sci. Rev.*, page 128, Apr. 2011. doi:10.1007/s11214-011-9774-z.
- Y. Narita and S. P. Gary. Inertial-range spectrum of whistler turbulence. *Annales Geophysicae*, 28:597–601, Feb. 2010. doi:10.5194/angeo-28-597-2010.
- J. J. Podesta and S. P. Gary. Magnetic Helicity Spectrum of Solar Wind Fluctuations as a Function of the Angle with Respect to the Local Mean Magnetic Field. *ApJ*, 734:15, June 2011. doi:10.1088/0004-637X/734/1/15.
- F. Sahraoui, M. L. Goldstein, G. Belmont, P. Canu, and L. Rezeau. Three Dimensional Anisotropic k Spectra of Turbulence at Subproton Scales in the Solar Wind. *Physical Review Letters*, 105(13):131101–+, Sept. 2010. doi:10.1103/PhysRevLett.105.131101.
- S. Saito, S. P. Gary, and Y. Narita. Wavenumber spectrum of whistler turbulence: Particle-in-cell simulation. *Physics of Plasmas*, 17(12):122316, Dec. 2010. doi:10.1063/1.3526602.
- C. S. Salem, G. G. Howes, D. Sundkvist, S. D. Bale, C. C. Chaston, C. H. K. Chen, and F. S. Mozer. Identification of Kinetic Alfvén Wave Turbulence in the Solar Wind. *ApJ*, 745:L9, Jan. 2012. doi:10.1088/2041-8205/745/1/L9.
- A. A. Schekochihin, S. C. Cowley, W. Dorland, G. W. Hammett, G. G. Howes, E. Quataert, and T. Tatsuno. Astrophysical Gyrokinetics: Kinetic and Fluid Turbulent Cascades in Magnetized Weakly Collisional Plasmas. *Astrophys. J. Suppl. Ser.*, 182:310–377, May 2009. doi:10.1088/0067-0049/182/1/310.
- C. W. Smith, K. Hamilton, B. J. Vasquez, and R. J. Leamon. Dependence of the Dissipation Range Spectrum of Interplanetary Magnetic Fluctuations on the Rate of Energy Cascade. *Astrophys. J. Letters*, 645:L85–L88, July 2006. doi:10.1086/506151.
- C. W. Smith, B. J. Vasquez, and J. V. Hollweg. Observational Constraints on the Role of Cyclotron Damping and Kinetic Alfvén Waves in the Solar Wind. *ApJ*, 745:8, Jan. 2012. doi:10.1088/0004-637X/745/1/8.
- O. Stawicki, S. P. Gary, and H. Li. Solar wind magnetic fluctuation spectra: Dispersion versus damping. *J. Geophys. Res.*, 106: 8273–8282, May 2001. doi:10.1029/2000JA000446.
- C. Torrence and G. P. Compo. A Practical Guide to Wavelet Analysis. *Bulletin of the American Meteorological Society*, 79:61–78, Jan. 1998.

We thank the referee for constructive comments. We are also grateful to G. Howes for useful indications. We thank the team of Cluster Active Archive. This work was partly supported by the Centre National d’Etudes Spatiales (CNES) and Program National Soleil–Terre (PNST/INSU).